Bandgap Opening in Graphene Antidot Lattices: The Missing Half

Fangping Ouyang,[†,‡] Shenglin Peng,[‡] Zhongfan Liu,[†,*] and Zhirong Liu[†,*]

[†]College of Chemistry and Molecular Engineering, State Key Laboratory for Structural Chemistry of Unstable and Stable Species, and Beijing National Laboratory for Molecular Sciences (BNLMS), Peking University, Beijing 100871, China, and [‡]School of Physics Science and Technology, Central South University, Changsha 410083, China

ABSTRACT The electronic structure of graphene antidot lattices (GALs) with zigzag hole edges was studied with first-principles calculations. It was revealed that half of the possible GAL patterns were unintentionally missed in the usual construction models used in earlier studies. With the complete models, the bandgap of the GALs was sensitive to the width *W* of the wall between the neighboring holes. A nonzero bandgap was opened in hexagonal GALs with even *W*, while the bandgap remained closed in those with odd *W*. Similar alternating gap opening/closing with *W* was also demonstrated in rhombohedral GALs. Moreover, analytical solutions of single-walled GALs were derived based on a tight-binding model to determine the location of the Dirac points and the energy dispersion, which confirmed the unique effect in GALs.

KEYWORDS: graphene · antidot lattices · bandgap · electronic structure · first-principles calculations · tight-binding model

Undoubtedly, graphene is currently one of the hottest materials in nanoscience and nanotechnology.[1] It possesses great potential applications in many emerging areas such as next-generation ultrahigh performance electronics and transistor logic circuits, sensors, and transparent conductors.[2−4] Several schemes have been proposed to open a tunable bandgap in graphene, which is required for semiconductor materials.[2,5−8] Recently, a strategy of constructing periodic holes on graphene to form graphene antidot lattices (GALs) has been extensively studied.[9−15] Theoretical calculations have predicted that antidot lattices change the electronic properties of graphene from semimetallic to semiconducting, where the opened gap can be tuned by the size, shape, and symmetry of both the hole and the lattice cell.[9−13,16−19] The induced gap in GALs is approximately proportional to the hole diameter and inversely proportional to the superlattice cell area, so one can achieve a substantial gap value of ~0.2 eV in a unit cell of 10 nm.[9] Accordingly, the transport properties of graphene nanoribbons (GNRs) are modulated by the existence of the antidots.[20−24] Antidot lattices on graphene also affect the occurrence of flat bands and collective magnetic behavior, and thus may lead to applications in storage media and spintronics.[9,10,25−30] Alternative periodic perturbations by such means as selective adsorption and nanohubs have also been explored theoretically.[31−43]

Essential experimental progresses of GALs have been achieved. Graphene films with hole diameters of 20−150 nm and cell sizes of 35−400 nm have been successfully fabricated *via* electron beam lithography, block copolymer lithography, and self-assembling of monodisperse colloidal microspheres.[14,15,44−46] Chemical synthesis has been used to produce subnanometer holes and periodicity (porous graphenes), which could be used as atmospheric nanofilters.[47−49] Effects such as Aharonov−Bohm oscillations, weak localization, and stiffening in Raman spectroscopy have been detected on GALs. Some studies have demonstrated that GALs have an effective energy gap of 100 meV and an ON−OFF ratio up to 10, which suggests the promising value of the scheme of GALs.[15,46] A bandgap was also successfully opened in graphene using an alternative approach of patterned hydrogenation.[50]

On examining the published theoretical works of GALs in the literature, we noticed that a half of the possible GALs patterns were unintentionally missed. For example, the unit cell of hexagonal GALs (Figure 1) was usually characterized by the side length *L*, which is equal to the number of the outermost carbon atoms on each side (*L* = 3 in Figure 1a). To shrink or expand the unit cell, one usually removed the outermost zigzag carbon chains or added extra chains outside the cell. This decreases or increases *L* by 1, and thus *L* is an integer.[9,29] However, when the lattices that are formed after assembling the cells (Figure 1b,c) are inspected, it can be seen that the width *W* of the wall between the nearest-neighboring holes changes incrementally by 2. With the above approach, only even values of *W* are

* Address correspondence to zfliu@pku.edu.cn, LiuZhiRong@pku.edu.cn.

Received for review February 13, 2011 and accepted April 22, 2011.

Published online April 22, 2011
10.1021/nn200580w

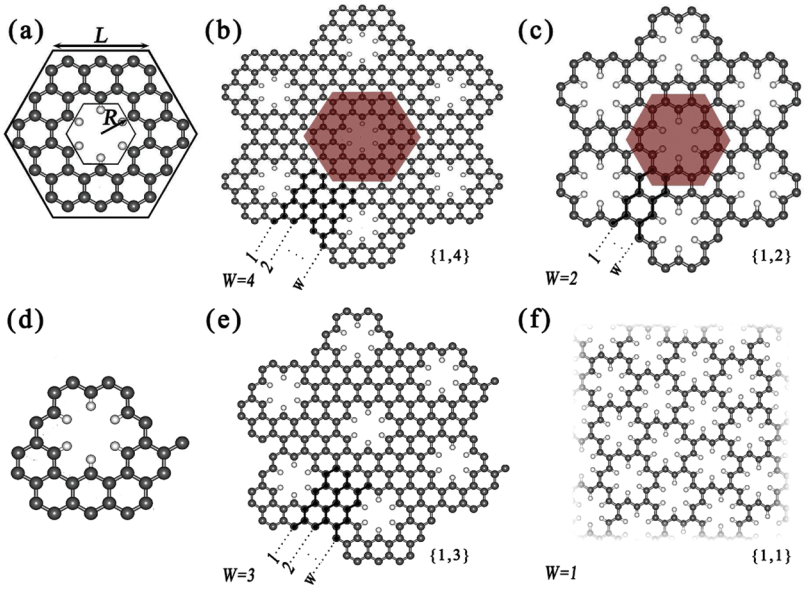

Figure 1. Hexagonal GALs with even and odd wall width *W*. The gray and white balls represent carbon and saturated hydrogen atoms, respectively. (a) A hexagonal unit cell which is characterized by a side length *L* = 3 and a hole radius *R* = 1. (b) The assembly of the unit cells in panel a, resulting in a wall width of *W* = 4. A unit cell is highlighted by shading. (c) Unit cells with *L* smaller than those in panels a and b by 1 (*L* = 2) give a *W* smaller by 2 (*W* = 2). (d) A unit cell and (e) its assembly into a lattice with an odd wall width of *W* = 3. (f) GALs composed of connected single carbon chains, which have the smallest wall width of *W* = 1. The systems are designated by the notation {*R*, *W*}.

considered while the other half (odd *W* values, see Figure 1d–f) are overlooked.[9–11,13,29] This is particularly apparent for GALs at the extreme end, such as those composed of connected single carbon chains with an odd *W* of 1 (Figure 1f) which are of interest for their theoretical simplicity (as will be shown below) and their close relation to the carbon atomic chains.[51,52] In this paper, we calculated the electronic structure of GALs using density functional theory (DFT) to investigate the different effects of odd and even *W*. GALs with odd *W* (Figure 1) were found to have unique properties, such as the bandgap remaining closed.

RESULTS AND DISCUSSION

We considered the graphene hexagonal antidot lattices (GHALs) as shown in Figure 1. Hexagonal holes with zigzag edges are created. Each system is designated by the hole radius *R* and the wall width *W*, as {*R*, *W*}. Unlike samples with circular holes,[9] *R* is measured in a unit as the number of the removed hexagonal carbon chains. So *R* is an integer and it is related to the number of removed carbon atoms ($N_{removed}$) by $N_{removed} = 6R^2$. We calculated the electronic structure of the GALs using the VASP code within the generalized gradient approximation (GGA).[53] Technical details are provided in the Methods section. The band structures of the GHALs with even and odd *W* are illustrated in Figure 2 for fixed holes of *R* = 1. With even *W*, the patterning of periodic holes opened a substantial bandgap around the Fermi level (Figure 2a). For example, the bandgap of the {1, 2} GHAL was 1.55 eV, and this decreased as the unit cell became larger. These results are consistent with previous studies.[9–11,29] However, with odd *W*, the GHALs displayed semimetallic behavior similar to pristine graphene, where the conduction band intersects the valence band at the *K*-points (Figure 2b). So, GHALs with odd *W* are incapable of opening a bandgap, which was never recognized before. The different effects of even and odd *W* are clearly demonstrated when the bandgap is shown as a function of *W* (Figure 2c). The bandgap alternates in a zigzag pattern with *W*. Experimental results for GALs suggested that they were semiconductors.[15,46] This controversy between theory and experiment is similar to that in graphene nanoribbons,[2,54,55] where only semiconductors were detected in experiments while both semiconductors and semimetals were predicted. The origin of the controversy may include the lack of precise edge control in device fabrication[55] and the influence of spontaneous edge-defect formation.[56] We also compared the relative stability of patterns with various *W* (Figure 2d). It showed that the curve of energy for odd *W* is overlapped with that for even *W*, so patterns with odd and even *W* are both likely to form in actual fabrications.

The bandgaps of GHALs with $R \leq 6$ and $W \leq 10$ were systematically calculated, and an analysis is given in Figure 3. The bandgaps of GHALs with odd *W* were all zero. For systems with even *W*, the bandgap decreased with increasing *W* (Figure 3a), but it showed a nonmonotonic dependence on *R* (Figure 3b). Pedersen *et al.* presented the following simple scaling rule for the bandgaps of circular GALs:[9]

$$E_g \propto \frac{N_{removed}^{1/2}}{N_{total}} \quad (1)$$

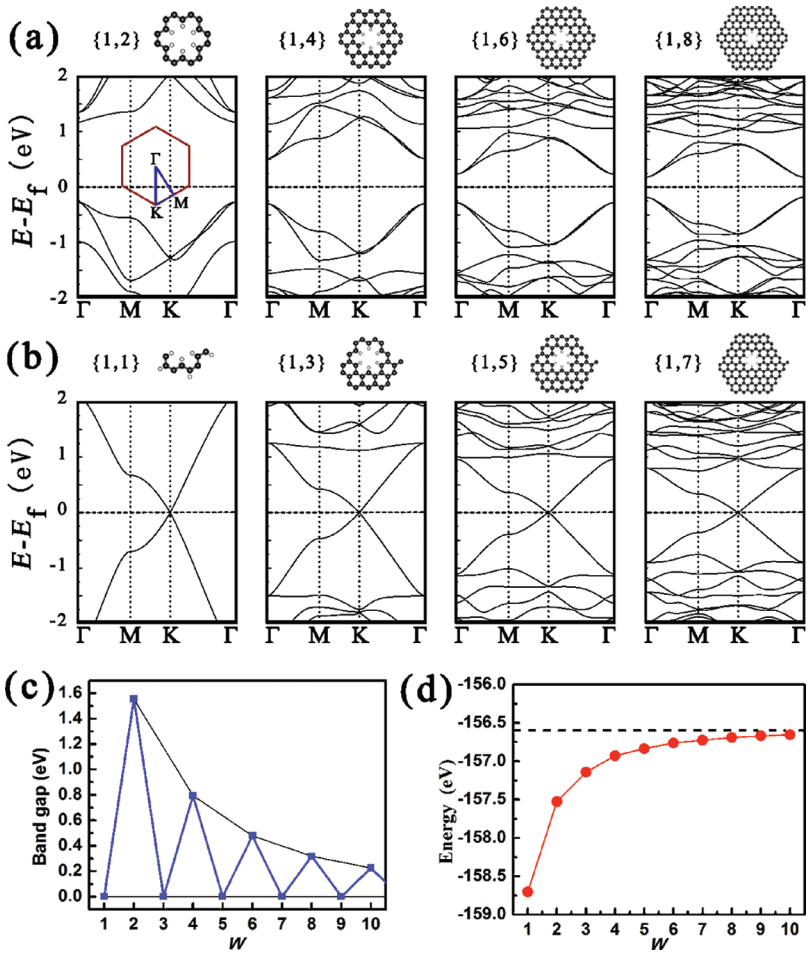

Figure 2. Effects of the wall width *W* on the electronic structure of GHALs with *R* = 1. (a,b) Energy band structures of the GHALs with even (a) and odd (b) *W*. The system notion {*R*, *W*} and the atomic structures of unit cell are shown at the top of the panels. The Fermi level is indicated with a black dashed line. (c) The bandgap of GHALs as a function of *W*. (d) The energy (per C atom) of GHALs as a function of *W*. The dashed line indicated the corresponding value of the pristine graphene.

where N_{total} is the total number of carbon atoms in the unit cell before the hole is made, and $N_{removed}$ is the number of removed carbon atoms. The scaling rule was also validated by Liu *et al.* for triangular and rhombus holes.[17] In our case, a description of E_g with eq 1 was not satisfactory (inset of Figure 3c). To better describe the E_g values, we introduced an exponential function into eq 1, and the numerical fitting gives

$$E_g = 19.45\exp(-14.57N_{total}^{-0.917} - 47.50C_{removed}^{1.140} + 51.54N_{total}^{-0.029}C_{removed}^{1.094})\frac{N_{removed}^{1/2}}{N_{total}} \quad (2)$$

where $C_{removed} = N_{removed}/N_{total}$ is the ratio of the removed carbon atoms. Equation 2 described the calculated E_g values well (Figure 3c). For large structures (large N_{total}), the asymptotic scaling of eq 2 converged to the earlier law of eq 1.

Recently, Clar sextet theory was applied to analyze the gap opening/closing of GALs and it was proposed that the number of sextets for patterns with a large bandgap was larger than one-third of the total number of hexagons.[57] However, we find that this rule is not applicable to GHALs we studied here. For a GHALs pattern {*R*, *W*}, there are *R* hexagons on the zigzag edge of each side, and at most one of them can be assigned to be sextet, so the ratio of sextet among hexagons is low although the gap may be opened. For example, the sextet ratio of the GHALs {3,2} is $^3/_{11}$, less than one-third, but the opened gap is as large as 0.73 eV.

Bandgap closing and the energy dispersion near the Fermi level of GHALs can be understood through the analytical solution of a Hückel tight-binding (TB) model for the extreme single-walled cases (*W* = 1). Under the TB framework, only the topological connection (bonding) between carbon atoms is important, so the unit cell of the single-walled GHALs can be generally described by a topological structure shown in Figure 4a. It is composed of three interconnected carbon chains, each of which contains *n* carbon atoms. For pristine graphene *n* = 2. The hole size *R* of the single-walled GHALs is related to *n* by $n = 2R + 2$ when *n* is even (see Figure 4b for an example of *n* = 4). We also considered the cases of odd *n* (see Figure 4c for *n* = 5). The holes with odd *n* are not exactly hexagonal in real space since they are

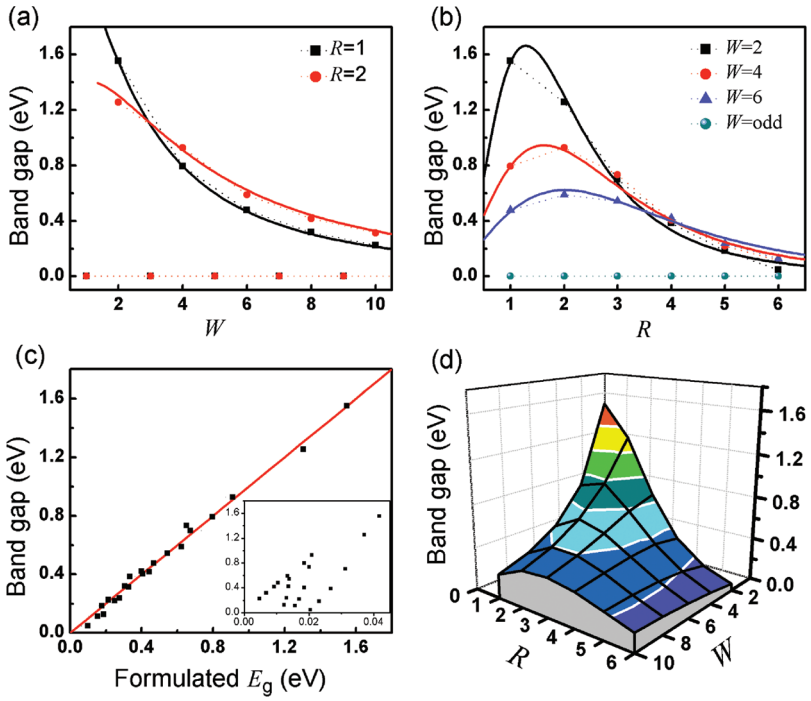

Figure 3. Bandgaps of GHALs. (a) The bandgap as a function of W with $R = 1$ and $R = 2$. (b) The bandgap as a function of R for various W values. Symbols in panels a and b are data points from DFT calculations, and solid lines are global fitting curves obtained with eq 2. (c) Comparison between bandgaps of GHALs with even W from DFT calculations and the formulated (fitting) values of eq 2. The inset presents the comparison with eq 1. (d) The bandgaps as functions of R and W.

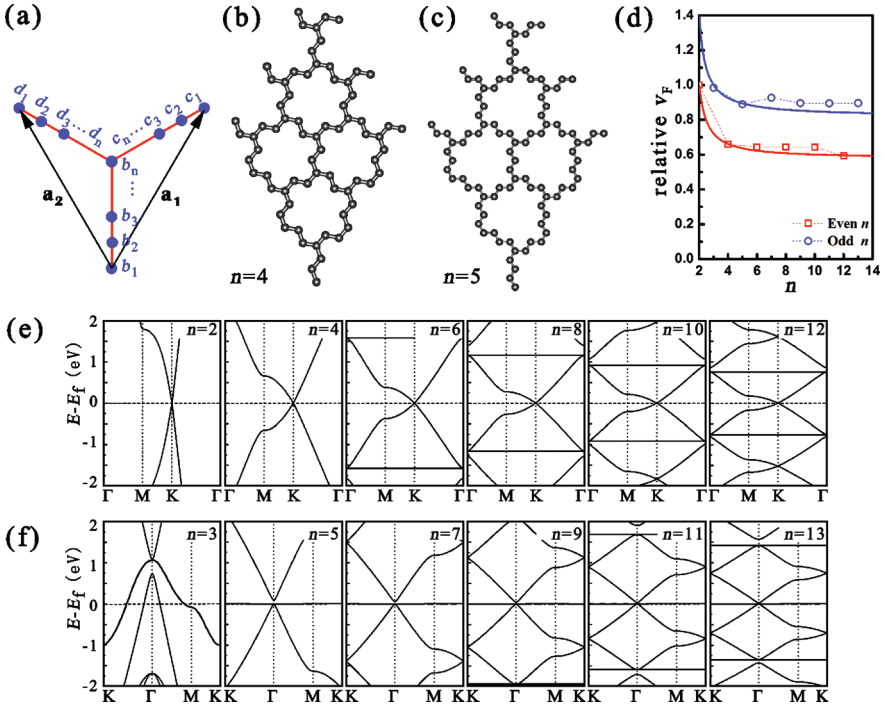

Figure 4. Analysis of the single-walled GHALs. (a) Topological structure of the unit cell of single-walled GHALs with n carbon atoms on each side edge of the hexagon; a_1 and a_2 denote the basic vectors. (b,c) Examples of single-walled GHALs with $n = 4$ and $n = 5$, respectively. Saturated hydrogen atoms are not shown. (d) The DFT calculated relative Fermi velocity $v_F(n)/v_F^{(0)}$ (symbols) compared with the predicted values from eq 3 (solid lines). (e,f) The DFT band structures of the single-walled GHALs with even and odd n. The Fermi level is indicated by a horizontal dashed line.

centered at carbon atoms instead of the pristine hexatomic ring centers. It is recognized that $n = 3$ corresponds to the case with single vacancy defects. However, they are equivalently hexagonal under the TB framework and can be considered with the same theory and included into the family of single-walled GHALs. Both

the Dirac points and energy dispersion were determined analytically for single-walled GHALs with even and odd n (see Supporting Information for details). It was predicted that the bandgap would remain closed no matter whether n is even or odd, but the Dirac points were at the K points when n was even, while at the Γ point when n was odd. The energy dispersion would be isotropic and cone-like as with pristine graphene, and the Fermi velocity v_F would depend on n as follows:

$$v_F(n) = \begin{cases} \dfrac{\sqrt{1+3(n-1)^2}}{3n-4} v_F^{(0)}, & \text{(even } n\text{)} \\ \sqrt{\dfrac{2(n-1)}{3n-5}} v_F^{(0)}, & \text{(odd } n\text{)} \end{cases} \quad (3)$$

where $v_F^{(0)}$ is the Fermi velocity of the pristine graphene ($n = 2$). To verify the predictions, we calculated the DFT band structures of the single-walled GHALs (Figure 4e, f). As predicted, the systems remained gapless with the valence and conduction bands touching at K points for even n (Figure 4e). For odd n (Figure 4f), a flat band occurred at $E = 0$ (except the abnormal case of $n = 3$, which may be caused by interactions of three saturated hydrogen atoms in the single vacancy where they are very close to each other). This is consistent with our analytical solution as well as the general symmetry consideration on the bipartite lattice structure of graphene.[29,58] The valence band approaches the conduction band at the predicted Γ point, but leaves a small gap. The calculated dispersion was fitted with $E(k) = ((kv_F)^2 + (\Delta/2)^2)^{1/2}$ to extract the Fermi velocity v_F for odd n, and the numerical values and the predicted values from eq 3 were compared along with those for even n in Figure 4d. The agreement was excellent for both even and odd n.

Shima and Aoki investigated the electronic structure of systems with honeycomb symmetry and showed that the bipartite systems could be classified into semimetals and semiconductors with a simple criterion.[59] The qualitative property of the bandgap opening/closing of GHALs revealed above is consistent with their criterion. To clarify whether the sensitivity of the bandgap opening/closing with respect to W was generally applicable to other zigzag-edged GALs without honeycomb symmetry, we studied graphene rhombohedral antidot lattices (GRALs, Figure 5a) where both unit cells and holes are rhombohedral. Similar to the GHALs, the single-walled GRALs displayed semimetallic behavior with a gapless k-linear dispersion (Figure 5b). The Dirac points of the single-walled GRALs were alternately located at two positions when the hole size R increased. It is noted that the Dirac points do not coincide with those in GHALs (Figures 2 and 4). The TB analytical solution of single-walled GRALs (see Supporting Information) predicted the Dirac points were at $K/2$ when R was odd, while at K when R was even. The DFT numerical results on Dirac points are close to the TB predictions, with a small shift away from Γ (note that M is on the extension line of $\Gamma-K$ in the expanded Brillouin graphics).

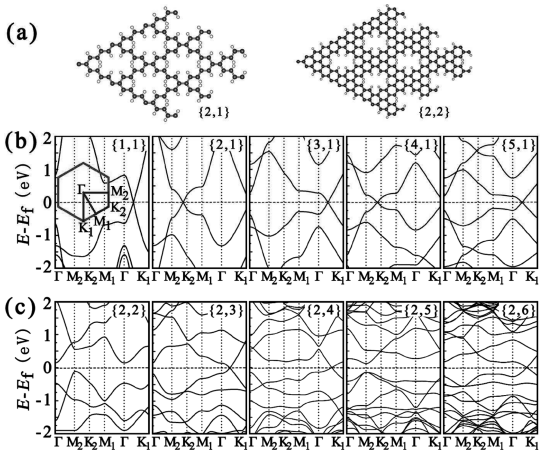

Figure 5. Atomic and band structures of GRALs. (a) Examples of GRALs which are characterized by the hole size R and the wall width W, $\{R, W\}$. (b) Energy band of single-walled GRALs with various R. (c) Effects of W on the energy band of GRALs when R is fixed as 2.

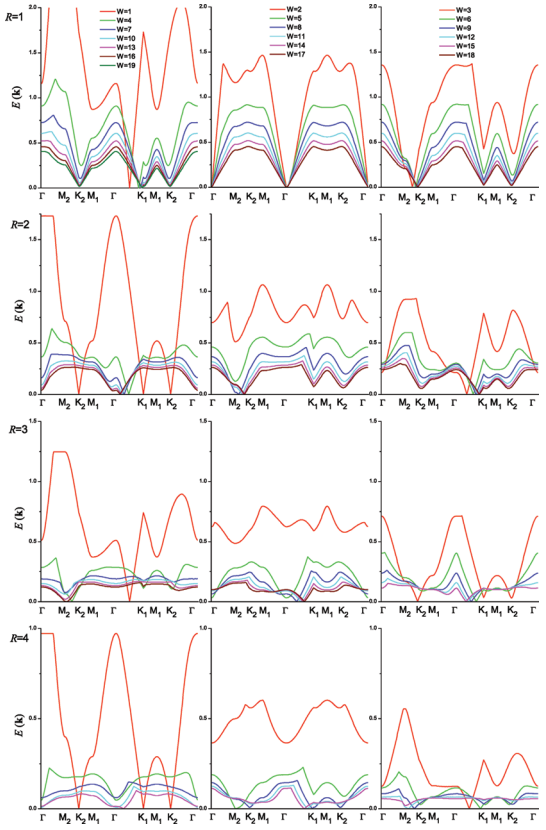

Figure 6. Band structures of GRALs obtained by numerically solving the TB model. The hopping parameter t_0 is 2.8 eV. $R = 1$, 2, 3, and 4 for panel lines from top to bottom. The left, middle, and right columns correspond to subgroups with $W = 3k + 1$, $3k + 2$, and $3k$, respectively. Only the conduction band is shown.

When W increased, the bandgap of the GRALs was opened and closed in a regular manner for the systems we examined. For example, the bandgap was opened for $W = 3k + 2$, while it was closed for $W = 3k$ or $3k + 1$ (Figure 5c). A further detailed calculation with a TB model

confirmed the existence of a period of $\Delta W = 3$ (Figure 6). When the spin polarization is considered, a further bandgap opening may be induced as shown by Liu *et al.*,[17] but this was not investigated in this paper. The existence of a period of three for the bandgap has been observed in armchair graphene nanoribbons (AGNRs) and GALs with armchair hole-edges when increasing the ribbon/wall width,[2,17,60] which originates from the discrete *k*-lines of the allowed electronic states of the armchair systems.[61] However, the period of three for the zigzag-edged GRALs cannot be explained by such a consideration because zigzag graphene nanoribbons (ZGNRs) are all metallic with edge states that are not dependent on the width.[62] So it is a novel property. The existence of the bandgap opening and closing also confirms the complexity of the electronic properties of GALs, which may have been missed in earlier studies.

CONCLUSIONS

In summary, first-principles calculations were used to study the electronic properties of zigzag-edged GALs and investigate the patterns that were missed in earlier studies. The general consensus has been that antidot patterning will open a bandgap in graphene. However, we found that a half of the possible GALs patterns were unintentionally neglected in earlier studies because of a problem with construction of the unit cell. Calculations on the complete set of hexagonal GALs showed that systems with even *W* were typical semiconductors, while those with odd *W* were semimetals with closed bandgaps as in pristine graphene. The sensitivity of the band structure with respect to *W* was also observed in rhombohedral GALs, which suggests this unique property is generally applicable. Analytical solutions for the single-walled GALs were obtained under a TB model to determine the location of the Dirac points and the energy dispersion near the Fermi level. The sensitive gap opening/closing revealed in our work may be useful for future design of GALs for their potential applications in graphene-based nanoelectronics.

METHODS

The structural optimizations and electronic structure calculations were performed using the Vienna *ab initio* simulation package (VASP),[53] which is based on density functional theory (DFT) and plane-wave pseudopotential method. The plane-wave cutoff energy is 400 eV for all calculations. The generalized gradient approximation (GGA)[63] and the Perdew-Burke-Ernzerhof (PBE) exchange-correlation function[64] are chosen. All geometry optimizations and electronic structure calculations are performed using periodic boundary conditions, and Brillouin-zone integrations are performed using a $11 \times 11 \times 1$ Monkhorst–Pach (MP) grid.[65] Criterion of convergence is selected that the residual forces are smaller than 0.01 eV/Å, and the change of total energy is smaller than 10^{-4} eV. To avoid the affect of layers, each graphene plane is separated by greater than 10 Å of vacuum in our calculation.

Acknowledgment. This work was supported by the National Natural Science Foundation of China (Grants Nos. 20973013 and 51072004), the Ministry of Science and Technology of China (Grants Nos. 2007CB936203 and 2011CB933003), the China Postdoctoral Science Foundation (Grant Nos. 20090460145 and 201003009), and the Fundamental Research Funds for the Central Universities.

Supporting Information Available: Additional computational details of the simulations, analysis of the tight-binding model, and calculation results. This material is available free of charge *via* the Internet at http://pubs.acs.org.

REFERENCES AND NOTES

1. Geim, A. K.; Novoselov, K. S. The Rise of Graphene. *Nat. Mater.* **2007**, *6*, 183–191.
2. Yan, Q. M.; Huang, B.; Yu, J.; Zheng, F. W.; Zang, J.; Wu, J.; Gu, B. L.; Liu, F.; Duan, W. H. Intrinsic Current–Voltage Characteristics of Graphene Nanoribbon Transistors and Effect of Edge Doping. *Nano Lett.* **2007**, *7*, 1469–1473.
3. Schedin, F.; Geim, A. K.; Morozov, S. V.; Hill, E. W.; Blake, P.; Katsnelson, M. I.; Novoselov, K. S. Detection of Individual Gas Molecules Adsorbed on Graphene. *Nat. Mater.* **2007**, *6*, 652–655.
4. Kim, K. S.; Zhao, Y.; Jang, H.; Lee, S. Y.; Kim, J. M.; Ahn, J. H.; Kim, P.; Choi, J. Y.; Hong, B. H. Large-Scale Pattern Growth of Graphene Films for Stretchable Transparent Electrodes. *Nature* **2009**, *457*, 706–710.
5. Duplock, E. J.; Scheffler, M.; Lindan, P. J. D. Hallmark of Perfect Graphene. *Phys. Rev. Lett.* **2004**, *92*, 225502.
6. Pereira, V. M.; Neto, A. H. C. Strain Engineering of Graphene's Electronic Structure. *Phys. Rev. Lett.* **2009**, *103*, 046801.
7. Li, Y.; Jiang, X. W.; Liu, Z. F.; Liu, Z. R. Strain Effects in Graphene and Graphene Nanoribbons: The Underlying Mechanism. *Nano Res.* **2010**, *3*, 545–556.
8. Guo, B. D.; Liu, Q.; Chen, E. D.; Zhu, H. W.; Fang, L.; Gong, J. R. Controllable N-Doping of Graphene. *Nano Lett.* **2010**, *10*, 4975–4980.
9. Pedersen, T. G.; Flindt, C.; Pedersen, J.; Mortensen, N. A.; Jauho, A. P.; Pedersen, K. Graphene Antidot Lattices: Designed Defects and Spin Qubits. *Phys. Rev. Lett.* **2008**, *100*, 136804.
10. Yu, D. C.; Lupton, E. M.; Liu, M.; Liu, W.; Liu, F. Collective Magnetic Behavior of Graphene Nanohole Superlattices. *Nano Res.* **2008**, *1*, 56–62.
11. Furst, J. A.; Pedersen, T. G.; Brandbyge, M.; Jauho, A. P. Density Functional Study of Graphene Antidot Lattices: Roles of Geometrical Relaxation and Spin. *Phys. Rev. B* **2009**, *80*, 115117.
12. Martinazzo, R.; Casolo, S.; Tantardini, G. F. Symmetry-Induced Band-Gap Opening in Graphene Superlattices. *Phys. Rev. B* **2010**, *81*, 245420.
13. He, H. Y.; Zhang, Y.; Pan, B. C. Tuning Electronic Structure of Graphene *via* Tailoring Structure: Theoretical Study. *J. Appl. Phys.* **2010**, *107*, 114322.
14. Eroms, J.; Weiss, D. Weak Localization and Transport Gap in Graphene Antidot Lattices. *New J. Phys.* **2009**, *11*, 095021.
15. Kim, M.; Safron, N. S.; Han, E.; Arnold, M. S.; Gopalan, P. Fabrication and Characterization of Large-Area, Semiconducting Nanoperforated Graphene Materials. *Nano Lett.* **2010**, *10*, 1125–1131.
16. Pedersen, T. G.; Flindt, C.; Pedersen, J.; Jauho, A. P.; Mortensen, N. A.; Pedersen, K. Optical Properties of Graphene Antidot Lattices. *Phys. Rev. B* **2008**, *77*, 245431.
17. Liu, W.; Wang, Z. F.; Shi, Q. W.; Yang, J. L.; Liu, F. Band-Gap Scaling of Graphene Nanohole Superlattices. *Phys. Rev. B* **2009**, *80*, 233405.

18. Furst, J. A.; Pedersen, J. G.; Flindt, C.; Mortensen, N. A.; Brandbyge, M.; Pedersen, T. G.; Jauho, A. P. Electronic Properties of Graphene Antidot Lattices. *New J. Phys.* **2009**, *11*, 095020.
19. Zhang, A. H.; Teoh, H. F.; Dai, Z. X.; Feng, Y. P.; Zhang, C. Band Gap Engineering in Graphene and Hexagonal BN Antidot Lattices: A First Principles Study. *Appl. Phys. Lett.* **2011**, *98*, 023105.
20. Zheng, X. H.; Zhang, G. R.; Zeng, Z.; Garcia-Suarez, V. M.; Lambert, C. J. Effects of Antidots on the Transport Properties of Graphene Nanoribbons. *Phys. Rev. B* **2009**, *80*, 075413.
21. Rosales, L.; Pacheco, M.; Barticevic, Z.; Leon, A.; Latge, A.; Orellana, P. A. Transport Properties of Antidot Superlattices of Graphene Nanoribbons. *Phys. Rev. B* **2009**, *80*, 073402.
22. Ritter, C.; Pacheco, M.; Orellana, P.; Latge, A. Electron Transport in Quantum Antidots Made of Four-Terminal Graphene Ribbons. *J. Appl. Phys.* **2009**, *106*, 104303.
23. Zhang, Y. T.; Li, Q. M.; Li, Y. C.; Zhang, Y. Y.; Zhai, F. Band Structures and Transport Properties of Zigzag Graphene Nanoribbons with Antidot Arrays. *J. Phys.-Condes. Matter* **2010**, *22*, 315304.
24. Ihnatsenka, S.; Zozoulenko, I. V.; Kirczenow, G. Band-Gap Engineering and Ballistic Transport in Edge-Corrugated Graphene Nanoribbons. *Phys. Rev. B* **2009**, *80*, 155415.
25. Ouyang, F. P.; Yang, Z. X.; Xiao, J.; Wu, D.; Xu, H. Electronic Structure and Chemical Modification of Graphene Antidot Lattices. *J. Phys. Chem. C* **2010**, *114*, 15578–15583.
26. Pereira, A. L. C.; Schulz, P. A. Additional Levels Between Landau Bands Due to Vacancies in Graphene: Towards Defect Engineering. *Phys. Rev. B* **2008**, *78*, 125402.
27. Chen, L.; Yu, D. C.; Liu, F. Magnetism in Nanopatterned Graphite Film. *Appl. Phys. Lett.* **2008**, *93*, 223106.
28. Yu, D. C.; Lupton, E. M.; Gao, H. J.; Zhang, C.; Liu, F. A Unified Geometric Rule for Designing Nanomagnetism in Graphene. *Nano Res.* **2008**, *1*, 497–501.
29. Vanevic, M.; Stojanovic, V. M.; Kindermann, M. Character of Electronic States in Graphene Antidot Lattices: Flat Bands and Spatial Localization. *Phys. Rev. B* **2009**, *80*, 045410.
30. Wu, D.; Yu, Z. M.; Xiao, J.; Ouyang, F. P. The Chemical Modification of Graphene Antidot Lattices. *Phys. E* **2010**, *43*, 33–39.
31. Park, P. S.; Kim, S. C.; Yang, S. R. E. Electronic Properties of a Graphene Antidot in Magnetic Fields. *J. Phys.-Condens. Matter* **2010**, *22*, 375302.
32. Park, C. H.; Yang, L.; Son, Y. W.; Cohen, M. L.; Louie, S. G. New Generation of Massless Dirac Fermions in Graphene under External Periodic Potentials. *Phys. Rev. Lett.* **2008**, *101*, 126804.
33. Tiwari, R. P.; Stroud, D. Tunable Band Gap in Graphene with a Noncentrosymmetric Superlattice Potential. *Phys. Rev. B* **2009**, *79*, 205435.
34. Du, A. J.; Chen, Y.; Zhu, Z. H.; Amal, R.; Lu, G. Q.; Smith, S. C. Dots *versus* Antidots: Computational Exploration of Structure, Magnetism, and Half-Metallicity in Boron–Nitride Nanostructures. *J. Am. Chem. Soc.* **2009**, *131*, 17354–17359.
35. Xu, B.; Lu, Y. H.; Feng, Y. P.; Lin, J. Y. Density Functional Theory Study of BN-Doped Graphene Superlattice: Role of Geometrical Shape and Size. *J. Appl. Phys.* **2010**, *108*, 073711.
36. Carara, S. S.; Batista, R. J. C.; Chacham, H. Modifications in Graphene Electron States Due to a Deposited Lattice of Au Nanoparticles: Density Functional Calculations. *Phys. Rev. B* **2009**, *80*, 115435.
37. Wu, X. J.; Zeng, X. C. Periodic Graphene Nanobuds. *Nano Lett.* **2009**, *9*, 250–256.
38. Guinea, F.; Low, T. Band Structure and Gaps of Triangular Graphene Superlattices. *Phil. Trans. R. Soc. A* **2010**, *368*, 5391–5402.
39. Casolo, S.; Martinazzo, R.; Tantardini, G. F. Band Engineering in Graphene with Superlattices of Substitutional Defects. *J. Phys. Chem. C* **2011**, *115*, 3250–3256.
40. Wang, L. G.; Chen, X. Robust Zero-Averaged Wave-Number Gap inside Gapped Graphene Superlattices. *J. Appl. Phys.* **2011**, *109*, 033710.
41. Zhang, A. H.; Dai, Z. X.; Shi, L.; Feng, Y. P.; Zhang, C. Energy-Gap Opening and Quenching in Graphene under Periodic External Potentials. *J. Chem. Phys.* **2010**, *133*, 224705.
42. Jiang, L. W.; Zheng, Y. S. Remarkable Enhancement of Terahertz Conductivity of Graphene Tuned by Periodic Gate Voltage. *Phys. Lett. A* **2010**, *375*, 203–207.
43. Chen, D. M.; Shenai, P. M.; Zhao, Y. Tight Binding Description on the Band Gap Opening of Pyrene-Dispersed Graphene. *Phys. Chem. Chem. Phys.* **2011**, *13*, 1515–1520.
44. Shen, T.; Wu, Y. Q.; Capano, M. A.; Rokhinson, L. P.; Engel, L. W.; Ye, P. D. Magnetoconductance Oscillations in Graphene Antidot Arrays. *Appl. Phys. Lett.* **2008**, *93*, 122102.
45. Heydrich, S.; Hirmer, M.; Preis, C.; Korn, T.; Eroms, J.; Weiss, D.; Schuller, C. Scanning Raman Spectroscopy of Graphene Antidot Lattices: Evidence for Systematic *p*-Type Doping. *Appl. Phys. Lett.* **2010**, *97*, 043113.
46. Sinitskii, A.; Tour, J. M. Patterning Graphene through the Self-Assembled Templates: Toward Periodic Two-Dimensional Graphene Nanostructures with Semiconductor Properties. *J. Am. Chem. Soc.* **2010**, *132*, 14730–14732.
47. Bieri, M.; Treier, M.; Cai, J. M.; Ait-Mansour, K.; Ruffieux, P.; Groning, O.; Groning, P.; Kastler, M.; Rieger, R.; Feng, X. L.; *et al*. Porous Graphenes: Two-Dimensional Polymer Synthesis with Atomic Precision. *Chem. Commun.* **2009**, *45*, 6919–6921.
48. Jiang, D. E.; Cooper, V. R.; Dai, S. Porous Graphene as the Ultimate Membrane for Gas Separation. *Nano Lett.* **2009**, *9*, 4019–4024.
49. Blankenburg, S.; Bieri, M.; Fasel, R.; Mullen, K.; Pignedoli, C. A.; Passerone, D. Porous Graphene as an Atmospheric Nanofilter. *Small* **2010**, *6*, 2266–2271.
50. Balog, R.; Jorgensen, B.; Nilsson, L.; Andersen, M.; Rienks, E.; Bianchi, M.; Fanetti, M.; Laegsgaard, E.; Baraldi, A.; Lizzit, S.; *et al*. Bandgap Opening in Graphene Induced by Patterned Hydrogen Adsorption. *Nat. Mater.* **2010**, *9*, 315–319.
51. Jin, C. H.; Lan, H. P.; Peng, L. M.; Suenaga, K.; Iijima, S. Deriving Carbon Atomic Chains from Graphene. *Phys. Rev. Lett.* **2009**, *102*, 205501.
52. Zanolli, Z.; Onida, G.; Charlier, J. C. Quantum Spin Transport in Carbon Chains. *ACS Nano* **2010**, *4*, 5174–5180.
53. Kresse, G.; Furthmuller, J. Efficiency of *ab-Initio* Total Energy Calculations for Metals and Semiconductors Using a Plane-Wave Basis Set. *Comput. Mater. Sci.* **1996**, *6*, 15–50.
54. Wang, X. R.; Ouyang, Y. J.; Li, X. L.; Wang, H. L.; Guo, J.; Dai, H. J. Room-Temperature All-Semiconducting sub-10-nm Graphene Nanoribbon Field-Effect Transistors. *Phys. Rev. Lett.* **2008**, *100*, 206803.
55. Han, M. Y.; Ozyilmaz, B.; Zhang, Y. B.; Kim, P. Energy Band-Gap Engineering of Graphene Nanoribbons. *Phys. Rev. Lett.* **2007**, *98*, 206805.
56. Li, J.; Li, Z. Y.; Zhou, G.; Liu, Z. R.; Wu, J. A.; Gu, B. L.; Ihm, J. S.; Duan, W. H. Spontaneous Edge-Defect Formation and Defect-Induced Conductance Suppression in Graphene Nanoribbons. *Phys. Rev. B* **2010**, *82*, 115410.
57. Petersen, R.; Pedersen, T. G.; Jauho, A. P. Clar Sextet Analysis of Triangular, Rectangular, and Honeycomb Graphene Antidot Lattices. *ACS Nano* **2011**, *5*, 523–529.
58. Inui, M.; Trugman, S. A.; Abrahams, E. Unusual Properties of Midband States in Systems with Off-Diagonal Disorder. *Phys. Rev. B* **1994**, *49*, 3190–3196.
59. Shima, N.; Aoki, H. Electronic-Structure of Superhoneycomb Systems—A Peculiar Realization of Semimetal Semiconductor Classes and Ferromagnetism. *Phys. Rev. Lett.* **1993**, *71*, 4389–4392.
60. Son, Y. W.; Cohen, M. L.; Louie, S. G. Energy Gaps in Graphene Nanoribbons. *Phys. Rev. Lett.* **2006**, *97*, 216803.
61. Mintmire, J. W.; Dunlap, B. I.; White, C. T. Are Fullerene Tubules Metallic. *Phys. Rev. Lett.* **1992**, *68*, 631–634.
62. Nakada, K.; Fujita, M.; Dresselhaus, G.; Dresselhaus, M. S. Edge State in Graphene Ribbons: Nanometer Size Effect and Edge Shape Dependence. *Phys. Rev. B* **1996**, *54*, 17954–17961.

63. Perdew, J. P.; Wang, Y. Accurate and Simple Analytic Representation of the Electron-Gas Correlation-Energy. *Phys. Rev. B* **1992**, *45*, 13244–13249.
64. Perdew, J. P.; Burke, K.; Ernzerhof, M. Generalized Gradient Approximation Made Simple. *Phys. Rev. Lett.* **1996**, *77*, 3865–3868.
65. Monkhorst, H. J.; Pack, J. D. Special Points for Brillouin-Zone Integrations. *Phys. Rev. B* **1976**, *13*, 5188–5192.